 CMES, vol.13, no.1, pp.35-47, 2006

A Frictionless Contact Algorithm for Meshless Methods

R. Vignjevic[1], T. De Vuyst[2] and J. C. Campbell[1]

Abstract: An approach to the treatment of contact problems involving frictionless sliding and separation under large deformations in meshless methods is proposed. The method is specially suited for non-structured spatial discretisation. The contact conditions are imposed using a contact potential for particles in contact. Inter-penetration is checked as a part of the neighbourhood search. In the case of conventional SPH contact conditions are enforced on the boundary layer 2h thick while in the case of the normalized SPH contact conditions are enforced for the particles lying on the contact surface. The implementation of the penalty based contact algorithm for the explicit time integration scheme is described and the performance of the new contact algorithm is illustrated with a number of examples.

keyword: Smooth particle hydrodynamics, SPH, Contact, Impact

1 Introduction

The analysis of contact problems raises great interest in several fields of research: metal forming, crashworthiness, projectile impact, impact on water, post-buckling response of structures. When considering these problems it is essential to use a space discretisation method capable of dealing with large deformations as well as a robust contact algorithm. When using particle (meshless) methods it is very difficult to define contact surfaces in a traditional manner such as used in FE. An efficient contact algorithm for meshless methods should be able to automatically update the interface geometry as it deforms. If one had to construct a surface around the SPH domain to consider contact then the benefit of using meshless methods for a large number of impact problems would be significantly reduced. The paper gives an outline for a frictionless contact algorithm for meshless methods.

[1] School of Engineering, Cranfield University, Bedfordshire MK43 0AL, UK
[2] Cenaero, Belgium

1.1 Contact Conditions

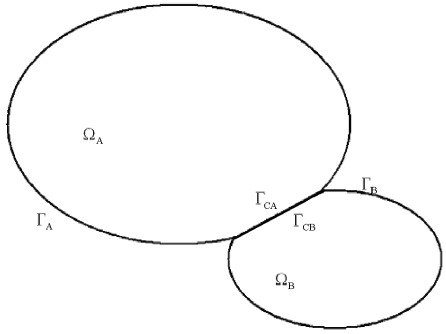

Figure 1 : Schematic representation of two bodies in contact.

Contact from a mathematical point of view is a constraint on the solution. The mathematical expressions for the constraints on the solution by the contact condition are commonly known as the Kuhn-Tucker conditions. In order to express these conditions mathematically we introduce a gap function, g, defined using closest point projection to determine pairs of points in contact that belong to body Ω_A and Ω_B and lie on their respective contact surfaces Γ_{CA} and Γ_{CB} (see Figure 1).

$$g = \hat{\mathbf{n}}_{\Gamma_{CA}} \cdot (\mathbf{x}_B - \mathbf{x}_A), \tag{1}$$

where $\mathbf{x}_A \in \Gamma_{CA}$ and

$$\mathbf{x}_B = \arg\ \min \|\mathbf{x}_A - \mathbf{x}\| \quad \forall \mathbf{x} \in \Gamma_{CB}. \tag{2}$$

In the case of frictionless contact, the only component of the contact force of interest is the component normal to the body, t_n. The Kuhn-Tucker Conditions can be written for this case as:

$$g \leq 0, \tag{3a}$$

$$t_{\mathbf{n}} \geq 0, \tag{3b}$$

$$g\, t_{\mathbf{n}} = 0. \tag{3c}$$

These conditions express the impenetrability, the compressive normal traction constraint, and the fact that the traction is only non-zero when $g = 0$.

If the rate of change of the gap function is written as $\dot{g}$, then the persistency of the contact, also known as the unitary contact condition, can be expressed as:

$$t_{\mathbf{n}} \cdot \dot{g} = 0 \tag{4}$$

If the equations of motion are expressed in the variational rate form the contact constraint used to impose the contact is:

$$\delta G = \delta G\,(t_n \cdot \dot{g}) = 0 \tag{5}$$

where δG is a (scalar) function of the contact persistency. This equation expresses the fact that the normal components of the contact forces do no work. Which is clear by noting that if the body is in contact and remains in contact then $\dot{g} = 0$, if the bodies are not in contact then $t_n = 0$.

Several studies and investigations have been carried out in order to achieve a general framework from which to derive a variational formulation for the contact problem [Laursen (2002), Wriggers (2002)] . These provide the necessary general background for contact modelling independent of the type of spatial discretisation [Simo and Tarnow (1992)]. To describe the general case of motion the equations of conservation of mass, conservation of linear momentum, the constitutive equation and the thermodynamic second law have to be integrated in time and space. Simo and Tarnow [Simo and Tarnow (1992)] demonstrated that the discrete form of the equations does not necessarily inherit the same conservative characteristics which, independently from the constitutive law, are intrinsic in the problem analysed. If the conservative nature of equations is preserved the scheme is called energy-momentum conserving.

Unfortunately, mathematically the contact conditions are not simple to enforce. In particular, the conditions to be imposed on the contact surface are neither Dirichelet nor von Neumann since both displacement and stress are unknown but related to each other through the Kuhn-Tucker conditions.

1.2 Contact in meshless methods

The contact boundary condition has been largely ignored in the conventional Smooth Particle Method (SPH), with contact between two bodies simply handled through the conservation equations. With this approach there is no restriction on particles from one body being treated as neighbour particles of a particle in another body. Interpolating over neighbour particles regardless of their material type is not only physically incorrect, but also results in mixing at the contact interface as SPH does not require the velocity field to be single valued at a point. Monaghan proposed a modification to the SPH method to prevent the interpenetration, which he called XSPH [Monaghan (1989)], where the velocity is single valued. While Monaghan's modification does prevent interpenetration it does nothing to solve two other problems with treating contact through the conservation equations:

- Generation of non-physical tensile forces, resisting separation of two bodies.
- Generation of shear stresses preventing friction-less or low friction sliding.

Several contact algorithms have been proposed for treatment of contact between particles and an FE mesh. Both Attaway et al. [Attaway and et al (1994)] and Johnson [Johnson (1994)] use a master slave algorithm and enforce the particleFE mesh contact constraint with the penalty method. While this method could be extended to work with SPH to SPH contact, the drawback is the necessity to define master and slave surfaces. This requires the determination of boundary particles, followed by the construction of a surface on the boundary nodes/particles. As connectivity varies in particle methods this process must be done repeatedly during a calculation.

Chen and Wang [Chen and Wang (2000)] use a similar node to surface contact detection method and use the mixed transformation or singular boundary kernel methods to enforce the contact condition. Again a major drawback is the need for a contact surface to be defined to calculate the penetration. The applications considered in this paper are metal forming (punch stretching and upsetting) where the nodes are in contact with a, assumed rigid, punch or die. This of course simplifies the definition of the master segments as they remain constant throughout the calculation. Gunther and Liu [Gunther and Liu (1998)] also use the mixed transformation method to model fluid-structure interaction.

The paper by Campbell, Vignjevic and Libersky [Campbell, Vignjevic and Libersky(2000)] describes the development and testing of a contact algorithm for SPH. The boundary is defined using the approach proposed by Randles and Libersky [Randles and Libersky (1996)]. After determining the boundary nodes a particle to particle penalty contact algorithm is used. This approach removes the need to define the material boundary as a line in 2D or a surface in 3D, but retains the need to identify boundary particles. This approach has many similarities with Belytschko's pinball contact algorithm [Belytschko and Neal (1991), Belytschko and Yeh (1993)]. However, due to non-uniqueness of the surface normal at vertices it was necessary to calculate two surface normals for each boundary particle, and detect a corner particle when the angle between the two normals exceeds a specified angle. The contact algorithm was tested for one and two dimensional problems for the velocity range between 0.2 and 4.0 km/s to determine the best penalty force equation and the best approach for applying the contact force. The examples used to demonstrate the performance of this technique were a flyer plate impact and the impact of two rubber balls.

The paper describes a new contact algorithm inspired by Monaghan's repulsive stress [Monaghan (2000)]. The new contact algorithm simplifies the calculation of direction of contact forces and avoids the problems related to non-uniqueness of the surface normal at particles. This is achieved by assigning a contact potential to all boundary particles and defining the contact force for particles in contact as the gradient of this field.

2 New Contact Algorithm

2.1 Contact Potential and Contact Force

The main problem in treating contact between bodies discretised with particles is defining the location of the boundary of the bodies. In an SPH approximation the particle position can be regarded as the centre of a subdomain with radius $2h$, where h is known as the smoothing length. Consequently the boundary is diffused over the distance of $2h$, where density varies smoothly from the material density, ρ, at the particle position to zero at the limit of the kernel support. In the case of corrected normalised (CN-SPH) [Campbell, Vignjevic and Libersky(2000)] the boundary coincides with the boundary particle locations.

Consider two particles A and B belonging to two different bodies, $\Omega_A$and $\Omega_B$respectively. Particle $B$is the closest member of Ω_B to particle A. In this case the gap function can be defined as:

$$\mathbf{g_n} = \left(\mathbf{x}^{(A)} - \mathbf{x}^{(B)}\right) \cdot \mathbf{n} \tag{6}$$

Where $\mathbf{x}^{(A)}$ and $\mathbf{x}^{(B)}$ are position vectors for particles A and B respectively and $\mathbf{n}$ is a unit vector normal to the contact surface at the location of particle A. In the new contact algorithm, instead of using the projection onto the direction of the normal a simplification is made and the actual distance between the particles is used to define the gap function,

$$g = \left\|\mathbf{x}^{(A)} - \mathbf{x}^{(B)}\right\| - (h^A + h^B). \tag{7}$$

Where $\| \cdot \|$ is a norm representing the distance between the two particles. The contact between two bodies occurs when the penetration g becomes > 0, i.e. the distance between the particles becomes smaller than two times the smoothing length. This is consistent with the SPH method.

Following the idea of body forces being defined as the gradient of a potential field [Zienkiewics (1991)], we use a similar approach to define contact forces. The contact potential function has to be carefully chosen in order to model contact between to bodies accurately. Intuitively one can see that the potential function should satisfy the following conditions:

- The potential should be zero in the interior of the domain.
- The potential should always be positive.
- The potential should become larger as the distance between to points decreases.

Defining the contact forces in this manner removes the need to determine and define the boundary surfaces of the two or more bodies and is more consistent with the basic SPH method. This is a critical consideration as although determining boundary particles has proved to be a tough problem, with no approach developed that works efficiently and reliably in 3D to track the evolving boundary in problems such as impact [Campbell, Vignjevic and Libersky(2000), Krongauz and Belytschko (1996), Randles and Libersky (1996)].

2.2 Contact initial boundary value problem

To consider the motion of two deformable bodies A and B in contact, one can start from the partial differential equations with the boundary and initial conditions (strong form of an initial boundary value problem), given below with respect to a current configuration.

$$\nabla \cdot \sigma + \rho \mathbf{b} = \rho \mathbf{a} \quad \text{in} \quad \Omega = \Omega_A \cup \Omega_B \quad , \tag{8a}$$

$$\sigma \cdot \mathbf{n} = \bar{\mathbf{t}} \quad \text{on} \quad \Gamma_t, \tag{8b}$$

$$\mathbf{u} = \bar{\mathbf{u}} \quad \text{on} \quad \Gamma_u, \tag{8c}$$

where $\mathbf{b}$ is the body force, $\mathbf{a}$ is the acceleration vector and $\bar{\mathbf{t}}$ is the external surface force with normal component t_N. With contact conditions:

$$\bar{\mathbf{t}}_A = -\bar{\mathbf{t}}_B \quad \text{on} \quad \Gamma_C = \Gamma_A \cap \Gamma_B \tag{9a}$$

$$\mathbf{t}_N \geq 0 \tag{9b}$$

$$g \leq 0 \tag{9c}$$

$$\mathbf{t}_N \cdot g = 0 \tag{9d}$$

where $\Gamma_t \cup \Gamma_{to} \cup \Gamma_u = \Gamma$, and $\Gamma_t \cap \Gamma_{to} = \emptyset$, $\Gamma_{to} \cap \Gamma_u = \emptyset$, $\Gamma_t \cap \Gamma_u = \emptyset$.

A weak form for the above initial boundary value problem is defined by choosing trial solution space U and a weighting space W for every moment in time within response time of interest.

$$U = \left\{ u : \Gamma \to R \,\middle|\, u \in H^1(\Omega), u = \bar{u} \quad \forall \mathbf{x} \in \Gamma_u \right\} \tag{10}$$

$$W = \left\{ w : \Gamma \to R \,\middle|\, w \in H^1(\Omega), w = u0 \quad \forall \mathbf{x} \in \Gamma_u \right\} \tag{11}$$

where: $H^1(\Omega)$ is Sobolev space of vector valued functions with square integrable derivatives.

Multiplication of the local equilibrium equation (8a) for the two bodies in contact by test/weighting function w gives:

$$\int_\Omega w \nabla \cdot \sigma \, dV = \int_\Omega w \rho (\mathbf{a} - \mathbf{b}) \, dV - \int_{\Gamma_c} w \bar{\mathbf{t}} d\Gamma, \tag{12}$$

where σ is Cauchy stress and ρ is current density. The integration by parts of the left hand side yields

$$\int_\Omega \nabla \cdot (w\sigma) \, dV - \int_\Omega \nabla w \cdot \sigma \, dV = \int_\Omega w \rho (\mathbf{a} - \mathbf{b}) \, dV - \int_{\Gamma_c} w \bar{\mathbf{t}} d\Gamma. \tag{13}$$

Using the divergence theorem, boundary conditions and the fact that $w = 0$ on Γ_u, (13) can be written as

$$\int_{\Gamma_t} w \sigma \cdot n \, d\Gamma - \int_\Omega \nabla w \cdot \sigma \, dV = \int_\Omega w \rho (\mathbf{a} - \mathbf{b}) \, dV - \int_{\Gamma_c} w \bar{\mathbf{t}} d\Gamma. \tag{14}$$

This equation represents a weak form of the initial boundary value problem with contact. This equation can now be discretised in space yielding the familiar form:

$$\int_\Omega \rho \mathbf{N}^T \mathbf{N} \, dV \ddot{\mathbf{d}} + \int_\Omega \mathbf{B}^T \sigma \, dV \mathbf{d} - \int_\Omega \mathbf{N}^T \mathbf{b} \, dV - \int_{\Omega_{CBL}} \mathbf{N}^T \mathbf{b_c} \, dV - \int_{\Gamma_t \cup \Gamma_u} \left(\mathbf{N}^T \sigma \right) \cdot \mathbf{n} \, d\Gamma = 0. \tag{15}$$

where:

$w = \mathbf{N}\mathbf{d}$,

$u = \mathbf{N}\mathbf{d}$,

and $\mathbf{N}$ is an array of shape functions. In the SPH method $\mathbf{N}$ is written as:

$$N_{ij} = \frac{m_j}{\rho_j} \frac{W_j(x_i)}{\sum_{j=1}^{np} W_j(x_i)} \tag{16}$$

I = particle at which shape function is evaluated,

J = particle around which the shape function is centred,

Np = number of neighbours for the i particle,

d = nodal displacement vector,

W = SPH kernel function. Throughout this paper this is the B-spline kernel.

Note that the surface integral in (14) has been substituted by a volume integral over the volume of the contact boundary layer, Ω_{CBL}, for the SPH formalism. This is due to the diffused nature of boundary in the conventional SPH algorithm and represents the material within the support distance of the contact boundary $\mathbf{b}_c$. The contact force is now defined as:

$$\mathbf{f_c} = \int_{\Omega_{CBL}} \mathbf{N}^T \mathbf{b_c} dV \tag{17}$$

This far, the nature of the force $\mathbf{b}_c$ has not been discussed in detail. Having in mind the requirements of the contact potential it is clear that the artificial stress introduced by Monaghan [Monaghan (2000)] to prevent tensile instability could be a good starting point. The artificial stress is a term that increases as the separation between the two particles i and j decreases and modifies the SPH momentum equation as follows:

$$\frac{\partial v_i}{\partial t} = -\sum_j m_j \left(\frac{p_j}{\rho_j^2} + \frac{p_i}{\rho_i^2} + R f_{ij}^n \right) \frac{\partial W_{ij}}{\partial x_i}, \tag{18}$$

where R is a scalar factor and:

$$f_{ij} = \frac{W(r_{ij})}{W(\Delta p_{avg})}. \tag{19}$$

Here Δp denotes the average particle spacing in the neighbourhood of particle i, and $r_{ij} = (x_i - x_j)/h$.

Following this approach the contact potential is defined as:

$$\phi(x_A) = \int_{\Omega_{CBL}} K \left(\frac{W(x_A - x_B)}{W(\Delta p_{avg})} \right)^n dV, \tag{20}$$

with $W(x_A - x_B) = 0$ if x_A and x_B belong to the same body. K is a user defined scalar contact stiffness penalty parameter. This integral can be approximated by point-wise integration as

$$\phi(x_i) = \sum_j^{NCONT} \frac{m_j}{\rho_j} K \left(\frac{W(r_{ij})}{W(\Delta p_{avg})} \right)^n. \tag{21}$$

The point-wise integration preserves the completely meshless character of the method. NCONT defines the list of neighbour particles that belong to a different body to particle i. A different numerical integration would require the definition of a boundary surface, which as mentioned earlier would result in a significant increase in complexity of the contact algorithm. Figure 2 shows how the contact potential varies with r_{ij}.

Using this contact potential the contact force can be defined as:

$$\begin{aligned} b_c(x_i) &= \nabla \phi(x_i) \\ &= \sum_j^{NCONT} \frac{m_j}{\rho_j} Kn \frac{W(r_{ij})^{n-1}}{W(\Delta p_{avg})^n} \nabla_{x_i} W(x_i - x_j). \end{aligned} \tag{22}$$

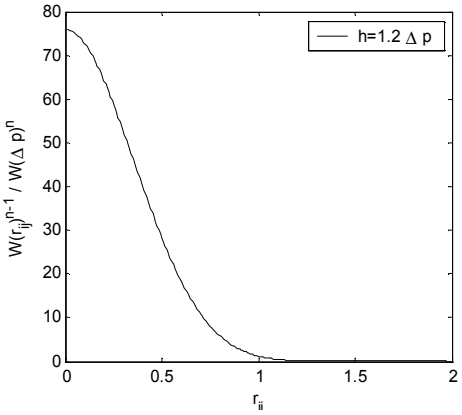

Figure 2 : Variation of contact potential with distance.

And finally the contact force vector can be evaluated by substituting Eq. 22 into Eq. 17:

$$\begin{aligned} \mathbf{f_c}(x_i) &= \int \mathbf{N_i^T} \mathbf{b_c}(x)\, dV \\ &= \int \mathbf{N_i^T} \left\{ \sum_l^{NCONT} \frac{m_l}{\rho_l} Kn \frac{W(r_{ij})^{n-1}}{W(\Delta p_{avg})^n} \nabla_{\mathbf{x}} W(x - x_l) \right\} dV. \end{aligned} \tag{23}$$

Which using after linearising and point-wise integration becomes:

$$\begin{aligned} \mathbf{f_c}(x_i) &= \int \mathbf{N_i^T} \mathbf{b_c}(x)\, dV \\ &= \mathbf{b_c}(x_i) \int \frac{m_i}{\rho_i} W(r_{ij})\, dV \\ &= \mathbf{b_c}(x_i) \frac{m_i}{\rho_i} \\ &= \sum_j^{NCONT} \frac{m_j}{\rho_j} \frac{m_i}{\rho_i} Kn \frac{W(r_{ij})^{n-1}}{W(\Delta p_{avg})^n} \nabla_{\mathbf{x_i}} W(r_{ij}). \end{aligned} \tag{24}$$

It is important to notice that direction of the contact force is determined by the SPH approximation of the gradient of the contact potential. For the conventional SPH method it is acting along the line connecting the pair of particles in contact and in the case of CN-SPH it has the direction of normal to the contact surface. The contact force is applied to boundary particles as soon as they get within $2h$ from each other, where h is the smoothing distance. The approach is in keeping with the meshless techniques in general and its implementation in 3D is not complex. The contact algorithm allows surfaces to come

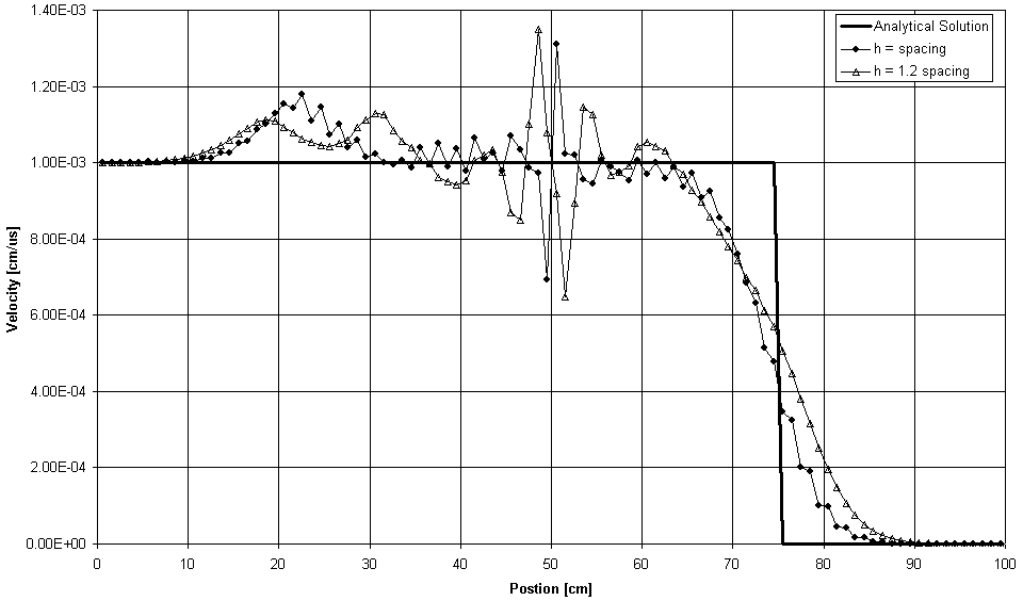

Figure 3 : Velocity Profile for Wave Propagation Problem, at time = 128.8μs.

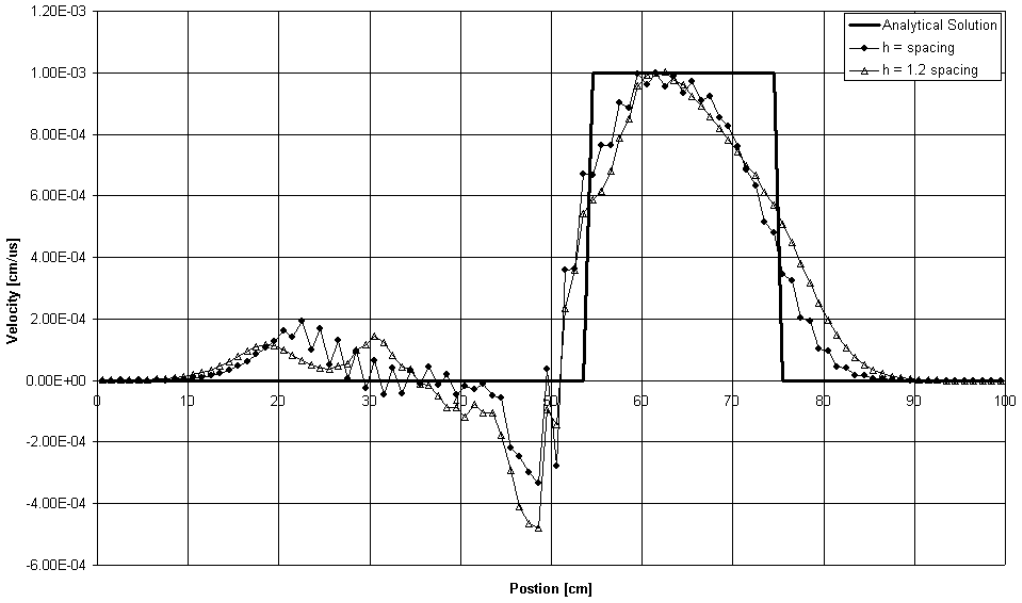

Figure 4 : Velocity Profile for Block Wave Propagation Problem, at time = 128.8μs.

together and separate in a physically correct manner. Furthermore this approach does not require the identification of boundary particles (hard to do robustly in 3D). The algorithm is numerically efficient because of its consistency with the general SPH approach and the fact that it utilises the already generated existing neighbour lists.

With respect to the variational consistency the contact force itself is derived using Galerkin method approach. No assumptions were made about the contact potential function except that it depends on the distance between the two bodies. The contact constraint is imposed directly through the shape functions of the particles in contact, which control the penalty stiffness at the same time. Within a time step contact forces are evaluated at the time of integration of constitutive equation i.e. $t = t_{n+\frac{1}{2}}$.

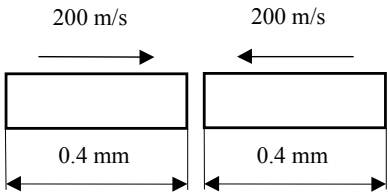

Figure 5 : Schematic representation of the 1D test problem

3 Numerical Examples

In order to test the performance of the contact algorithm a number of contact problems were analysed. The following analyses are described in detail: 1D wave propagation test, 1D bar impact, 2D plate impact, breaking dam in 2D, 3D hypervelocity impact.

3.1 1D Wave Propagation

This problem tests the ability of the contact algorithm to propagate a compressive wave across the contact interface, two versions of this problem are used. The first simply applies a fixed velocity to one side of a bar. The resulting stress wave is a step-function that travels through the bar. In the second version the prescribed velocity is only applied for a limited period of time. This results in a stress pulse (square wave) travelling through the bar. These tests are used in [Sauer (2000)] to test tied coupling between FE and SPH, along with a masterslave contact algorithm.

The problem consists of a steel bar 1 meter long split into two halves which interact thought the contact interface. The left end of the bar is given a prescribed velocity of 0.001 cm/μs. The material model is a linear elastic model with a Young's modulus of 2.1 Mbar, Poisson's ratio of 0.28 and density of 7.83 g/cm^3. The bar is discretised in 1D with 100 particles and the smoothing length is equal to the particle spacing. In the second case the prescribed velocity is only applied for 35μs.

The results of the wave propagation test are very similar to the results of the master-slave algorithm tested by Sauer [Sauer (2000)] (see Figure 3). The results also show the reflected wave observed by Sauer when using a standard master-slave algorithm. The reflected wave is slightly less pronounced with the contact algorithm based on a contact potential. Using a smoothing length equal to 1.2 times the particle spacing results in slightly smoother results. However in this case the oscillations at the contact surface are more pronounced.

The second test is identical in setup to the first test, but the prescribed velocity is set to 0 after 35μs. The results are shown in Figure 4. Again the results are similar to the ones reported in [Sauer (2000)].

These results show a similar accuracy compared to a standard masterslave penalty contact algorithm. However the main purpose of this contact algorithm is to use it to simulate impact problems mainly characterised by large displacements and deformations. The tests in this paragraph are wave propagation problems characterised by small deformations.

3.2 1D Bar Impact

The performance of the new contact algorithm can be further tested by simulating a 1D elastic bar impact. The aim of this was to further test the effectiveness of the contact force algorithm, in exclusion from any effect that could occur in 2D from the calculation of the vector along which the contact force was applied.

The test problem used was the impact of two 0.4 cm long bars, see Figure 5. The bar on the left-hand side was given material properties of steel, while the bar on the right-hand side was given material properties of aluminium. A total of 100 particles were placed along the 1D line, 50 particles in each bar. The smoothing length was 0.01 cm with the initial inter-particle space equal to the smoothing length. The space between the two end particles was 0.01, so there was no initial penetration. Each bar was given an equal but opposite initial velocity of 0.02 cm/μs.

To provide a reference point the problem was initially run without the contact algorithm, using the standard SPH kernel sums to allow interaction between the two bodies. This is shown in the figures as the no contact case. With the kernel sums the two end particles were initially in contact. Figures 6 and 7 shows the resulting stress and velocity profiles at time 48μs, and are in good agreement with the analytical solution. The stress waves are propagating away from the point of contact. At this point no significant differences can be seen between the two sets of results. Figure 8 shows the velocity profiles at time 300μs, with the profiles for kernel contact shown for comparison. At this point the release waves have reached the point of contact. One can see that with the contact algorithm, apart from a small elastic wave, the bars are

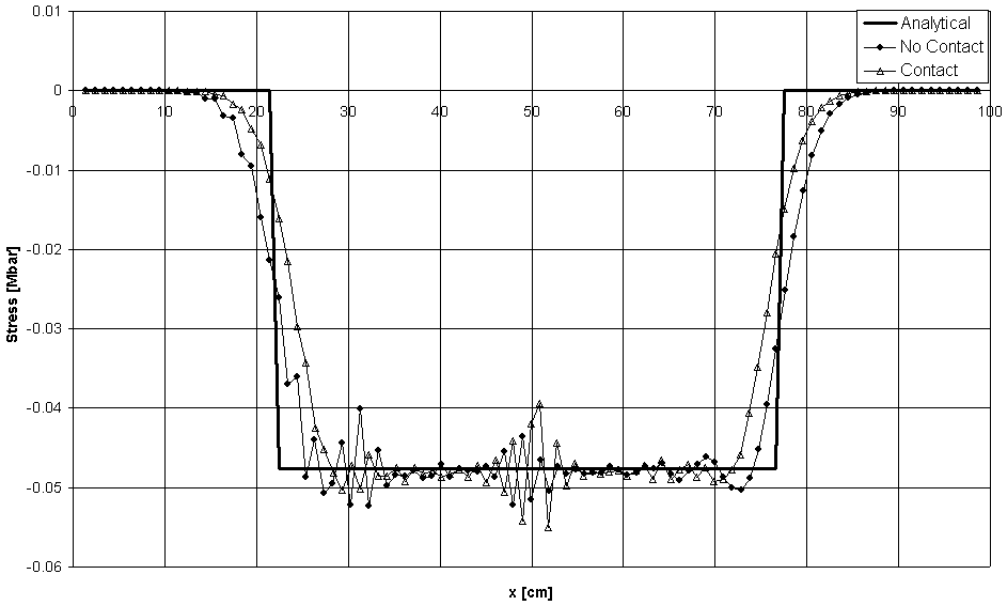

Figure 6 : Pressure profiles with and without contact at 48μs.

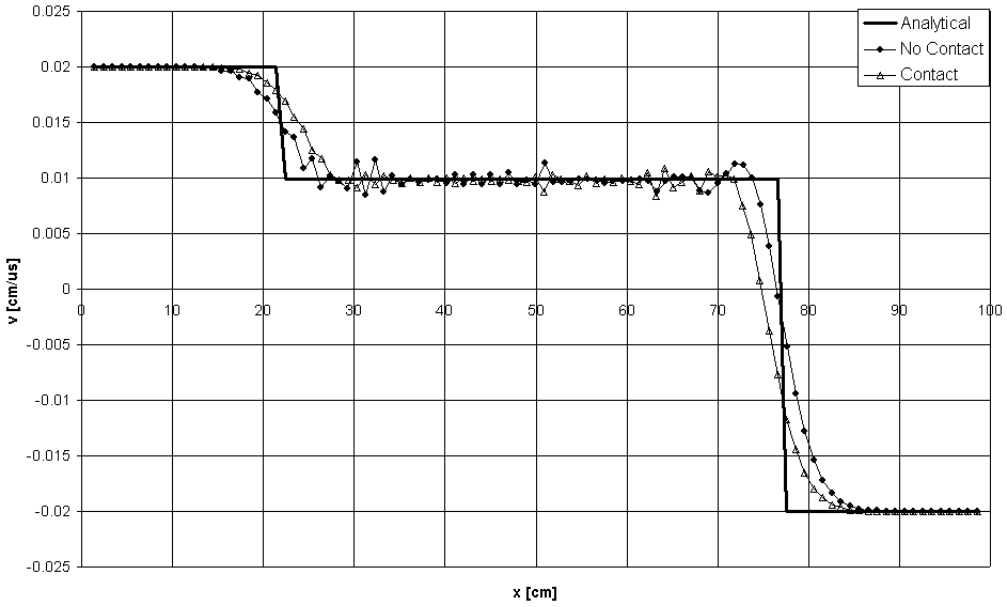

Figure 7 : Velocity profiles with and without contact at 48μs.

unloaded and no non-physical tensile stresses have been generated. This is in contrast with the use of kernel contact where non-physical tensile stresses and tensile instability around the point of contact develop, resulting in an error termination of the simulation around 270μs. From the velocity plot it can be seen that when the contact algorithm is used the bars are travelling away from each other with a speed almost equal and opposite to the initial impact speed. Considerable oscillation can be seen in the stress and velocity at the interface for kernel contact. This oscillation was described by Swegle [Swegle and et al (1996)] who observed it when modelling the 1D impact of two initially separated bodies using kernel contact. This oscillation corresponds to a zero energy mode, for which stress field does not cause particle accelerations that would reduce the stress amplitude. Swegle

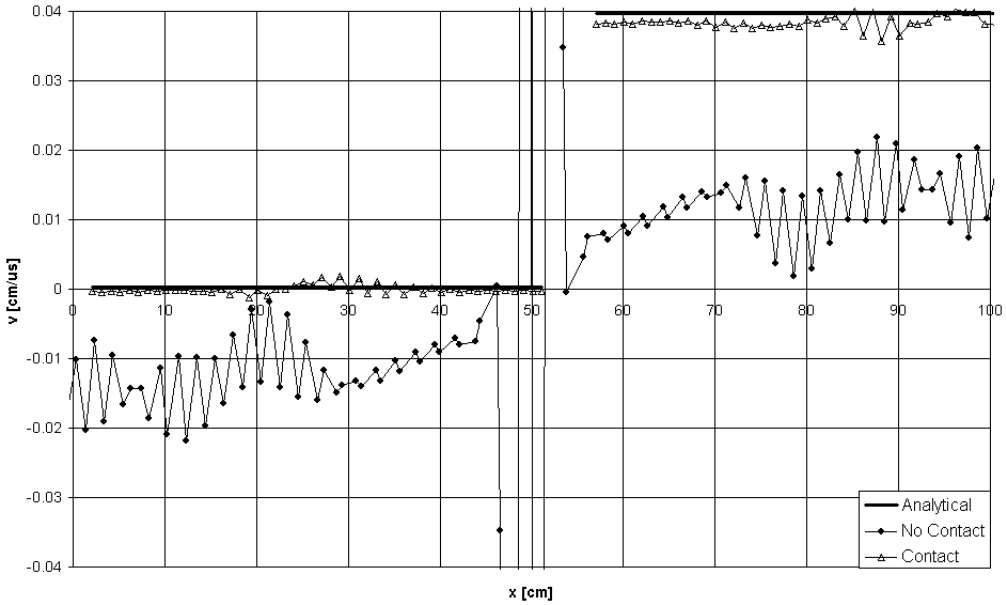

Figure 8 : Velocity profiles with and without contact at 300μs.

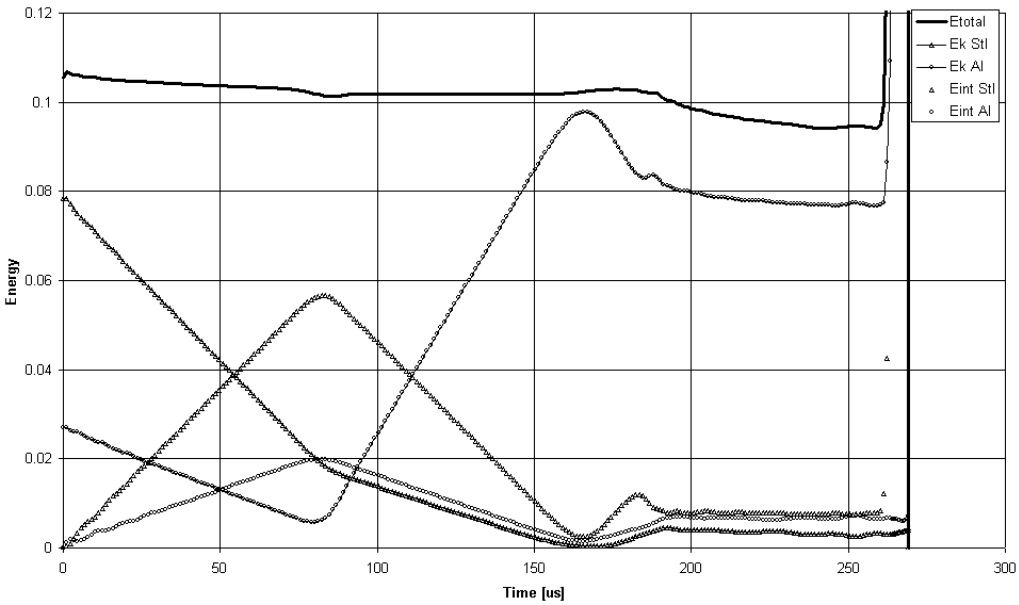

Figure 9 : Kinetic - and Internal Energy Time Histories without contact.

showed that this was a characteristic of the SPH method, as the SPH estimate to the stress field has its local maxima and minima at the particles giving the stress field gradient of zero. In the SPH method no acceleration will be produced at a particle if the stress at the two neighbour particles is equal, this is independent of the stress at the particle itself. This is the stress version of the SPH zero-energy mode where an alternating velocity field does not generate stresses in the material to resist the particle motion. Figure 9 and Figure 10 shows the exchange between kinetic - and strain energy as a function of time.

3.3 2D Plate Impact

As the 1D tests showed that the contact based on the contact potential performs satisfactorily, its performance was

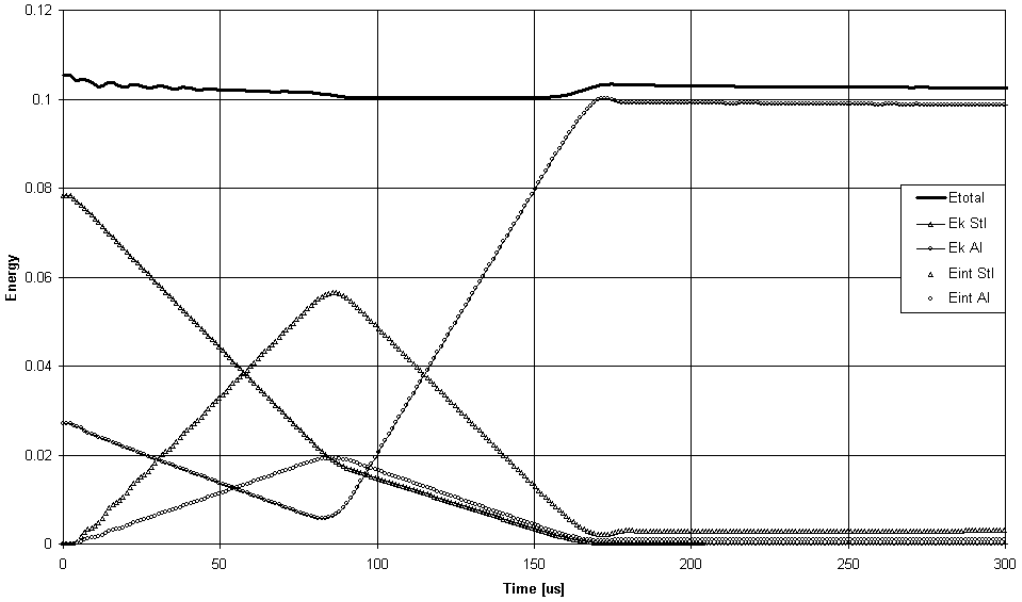

Figure 10 : Kinetic - and Internal Energy Time Histories with contact.

then tested in 2D. The contact algorithm was tested in 2D by modelling the normal symmetrical impact of two steel blocks, and a fluid sloshing simulation. The block impact test allows for the evaluation of the capability of the contact algorithm in dealing with corner contact, where at one side the material is in contact, and the other side is a stress-free surface. The fluid sloshing problem evaluates the ability to deal with frictionless sliding at the contact interface, and extreme deformations and change in contact surface.

For the symmetrical block impact each block was 1 cm by 0.4 cm and consisted of 50 particles by 20 particles, giving a total of 2000 particles in the whole model. The two blocks have an initial relative velocity of 0.04 cm/μs, see figure 11. The contact boundary particles in each body were initially spaced h apart, so the initial penetration was zero. The materials were modelled with an elastic-plastic material model, with material properties that are typical for steel.

The simulation results for this problem are shown in figure 12 to figure 13. Again the same simulation was performed without contact. These results are shown (on the LHS) for comparison. In figure 12 one can see the pressure in the blocks after 1μs. The block is at this point in compression, the release waves have not yet reached the centre of the block. From these results it is clear that the contact algorithm has no problems in dealing with contact on corners. In figure 13 the pressure in the blocks is shown just after the point where the release waves have reached the contact line (after 2μs). One can see the typical tensile stresses generated when no contact algorithm is used, while the results on the RHS show the beginning of the separation between the two unloaded blocks.

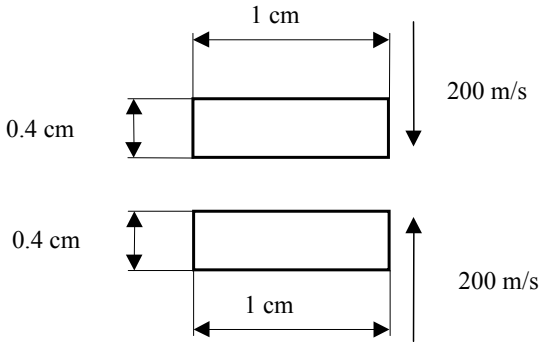

Figure 11 : Symmetric Block Impact in 2D: Problem Setup

3.4 Fluid Sloshing in 2D

The break simulation is the second 2D test that was performed. The test setup is identical to the experiment and simulation results reported in [Idelsohn, Storti and Onate (2001), Koshizuka, Nobe and Oka (1999)]. The dimensions of the container are 58.4cm long by 29.2cm high.

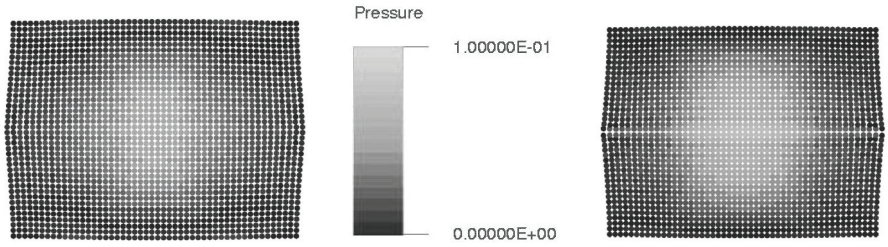

Figure 12 : Pressure plots 1μs after impact, without contact (LHS) and with contact (RHS)

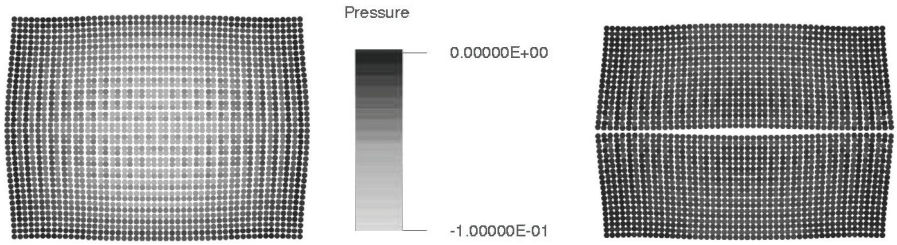

Figure 13 : Pressure plots 2μs after impact, without contact (LHS) and with contact (RHS)

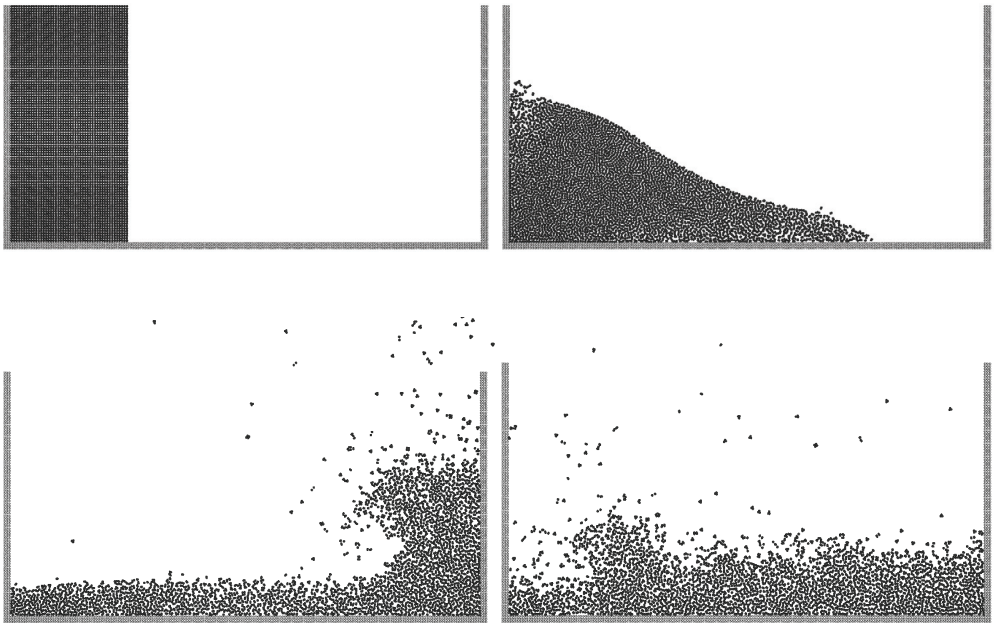

Figure 14 : Breaking Dam State Plots at 0.00, 0.20, 0.70, 1.00 s.

The volume of water is 14.6cm long by 29.2cm high. The fluid is modelled as a viscous fluid with the following equation of state to ensure that the material behaves quasi-incompressible:

$$p = B\left[\left(\frac{\rho}{\rho_0}\right)^{\gamma} - 1\right], \tag{25}$$

where B and γ are user defined constants. The volume

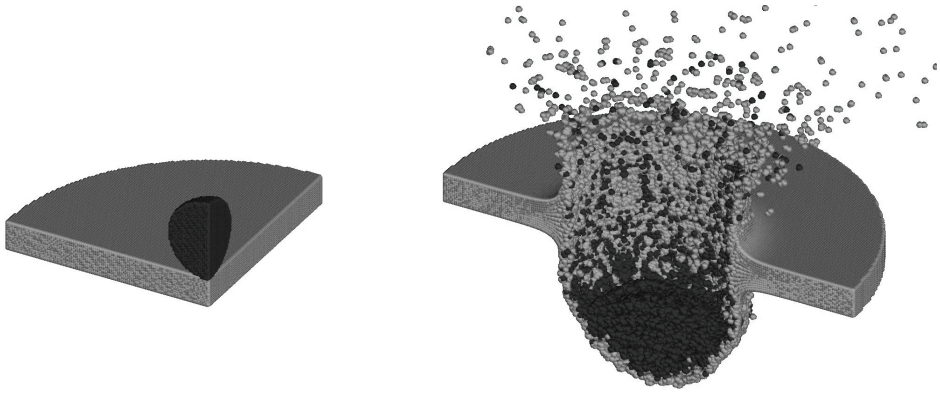

Figure 15 : Isometric View of 3D Hypervelocity Impact at 0.0 and 0.2μs.

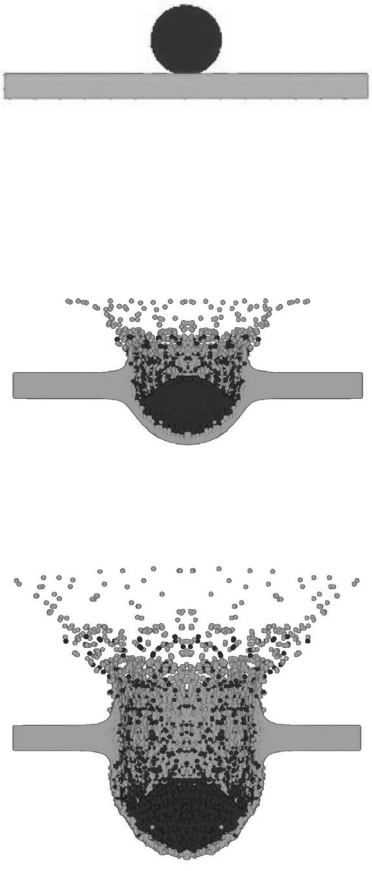

Figure 16 : Cross Section Plots of 3D Hypervelocity Impact at 0.0, 0.1 and 0.2μs.

of fluid is initially at rest and moves under the influence of a gravity field. The response time considered was 1.00s, and plots of the results are shown at 0.00, 0.20, 0.70 and 1.00s. The results, figure 14, compare well with the published experimental and simulation results [Idelsohn, Storti and Onate (2001), Koshizuka, Nobe and Oka (1999)].

3.5 3D Hypervelocity Impact

In order to demonstrate that this contact algorithm performs in 3D a hypervelocity impact of a sphere on a plate was simulated. This type of problem is a severe test for the robustness of the contact algorithm as both objects are subjected to extremely large deformations. The radius of the sphere is 0.3mm, the plate thickness and radius is 0.2mm and 0.15mm. The material of both objects is aluminium and an elasticplastic hydrodynamic material model with Gruneisen equation of state was used. The sphere has an initial velocity of 7km/s. Due to the symmetry of the problem a quarter model was created (see figure 15). Cross section plots after 0.0, 0.1 and 0.2μs are shown in figure 15 and figure 16. From these plots it can be seen that the algorithm does not cause any mixing of particles, even at very large deformations. No experimental data, such as hole diameter or debris cloud angle, was available to perform a more qualitative validation of the simulation results.

4 Conclusions

A conceptually simple and computationally efficient method for modelling contact in the SPH method has been proposed. The main advantages of this algorithm are:

The detection of contact and the calculation of the contact force are based on quantities that are already calculated within an SPH algorithm.

There is no need to construct contact surfaces, or to explicitly define normals to the surface and to calculate surface interpenetration.

The proposed approach can be used with the collocated and non-collocated normalised SPH method.

These features preserve the meshless nature of the solver. The new contact algorithm was successfully applied to several 1D, 2D and 3D problems. The results demonstrate the accuracy and robustness of the algorithm for a wide range of problems.

Acknowledgement: The work presented in this paper has been part funded by the CAST project. "CAST – Crashworthiness of Helicopters on Water: Design of Structures Using Advanced Simulation Tools" partially funded by the European Union under the Aeronautics part of the GROWTH RTD program (Contract G4RD-CT1999-01728).

References

Attaway, S.; Heinstein, M.; Swegle, J. (1994): Coupling of Smooth Particle Hydrodynamics with the Finite Element Method. *Nucl. Eng. Des. 150,* pp. 199-205.

Belytschko, T.; Neal, M. (1991): Contact-Impact By Pinball Algorithm With Penalty and Lagrangian Methods. *Int. J. Num. Meth. Engrg*. 31, pp. 547-572.

Belytschko, T.; Yeh, I. (1993): The splitting pinball method for contact-impact problems. *Comp. Methods Appl. Mech. Eng.* 105, pp. 375–393.

Campbell, J.; Vignjevic, R.; Libersky, L. (2000): A Contact Algorithm for Smoothed Particle Hydrodynamics. *Comp. Methods Appl. Mech. Eng. 184,* pp. 49-65.

Chen, J.; Wang, H. (2000) New Boundary Condition Treatments in Meshfree Computation of Contact Problems, *Comp. Methods Appl. Mech. Eng. 187,* pp. 441-468.

Gunther, F.; Liu, W. K. (1998): Implementation of Boundary Conditions for Meshless Methods. *Comp. Methods Appl. Mech. Eng. 163,* pp. 205-230

Idelsohn, S.; Storti, M.; Onate, E. (2001): Lagrangian Formulations to Solve Free Surface Incompressible Inviscid Fluid Flows. *Comput. Methods Appl. Mech. Engrg. 191,* pp. 583-593.

Johnson, G. (1994): Linking of Lagrangian particle methods to standard finite element methods for high velocity impact computations. *Nucl. Eng. Des. 150,* pp. 265-274.

Koshizuka, S.; Nobe, N.; Oka, Y. (1999): Moving Particle Semi-Implicit Method for Fragmentation of Incompressible Fluid. *Nucl. Eng. Sci, 129,* pp. 421-434.

Krongauz, Y.; Belytschko, T. (1996): Enforcement of Essential Boundary Conditions in Meshless Approximations using Finite Elements. Comput. Methods Appl. Mech. Engrg. 131, pp. 133-145.

Laursen, T. A. (2002): Computational Contact and Impact Mechanics, Springer.

Monaghan, J. J. (1989): On the problem of penetration in particle methods. *J. Comput. Phys. 82,* pp. 1–15.

Monaghan, J. (2000): SPH without a Tensile Instability. *J. Comput. Phys*. 159, pp. 290-311.

Randles, P.; Libersky, L. (1996): Smoothed particle hydrodynamics: Some recent improvements and applications. *Comp. Methods Appl. Mech. Engng. 139,* pp. 375-408.

Sauer, M. (2000): Adaptive Kopplung des Netzfreien SPH-Verfahrens mit Finiten Elementen zur Berechnung von Impaktvorgängen. *PhD Thesis, Universität der Bundeswehr München*

Simo, J.; Tarnow, N. (1992): The Discrete Energy-Momentum Method Conserving Algorithm for Nonlinear Elastodynamics. *Z. Angew. Math. Phys. 43.*

Swegle, J.; Attaway, S.; Heinstein, M.; Mello, F.; Hicks, D. (1996): An analysis of smoothed particle hydrodynamics. *Technical Report SAND93-2513, Sandia National Laboratories.*

Wriggers, P. (2002): Computational Contact Mechanics, John Wiley & Sons.

Zienkiewics, O. (1991): The Finite Element Method, McGraw Hill, London.